Nanoscale

PAPER

View Article Online
View Journal

Cite this: DOI: 10.1039/c4nr00761a

Revisiting the coordination chemistry for preparing manganese oxide nanocrystals in the presence of oleylamine and oleic acid†

Hongwei Zhang,[a] Lihong Jing,[a] Jianfeng Zeng,[a] Yi Hou,[a] Zhen Li*[b] and Mingyuan Gao*[a]

Received 11th February 2014
Accepted 31st March 2014

DOI: 10.1039/c4nr00761a

www.rsc.org/nanoscale

By pyrolyzing manganese(II) acetate in 1-octadecene in the presence of oleylamine and oleic acid, manganese oxide nanocrystals were prepared. It was observed that both MnO and Mn_3O_4 nanocrystals were simultaneously formed by quickly heating the reaction mixture up to 250 °C, while a preheating procedure carried out at 100 °C led to uniform MnO nanocubes that developed into eight-arm MnO nanocrystals upon prolonged reaction. To understand the mechanisms for forming these two different kinds of manganese oxide nanocrystals, *i.e.*, Mn_3O_4 and MnO, the coordination between oleic acid/oleylamine and Mn^{2+} was investigated. The detailed investigations suggest that Mn^{2+}–oleylamine coordination is kinetically driven and favorable for the formation of Mn_3O_4 nanocrystals due to the relatively low electronegativity of N from oleylamine, while Mn^{2+}–oleate coordination is thermodynamically driven and can prevent the central metal ion (Mn^{2+}) from being oxidized owing to the relatively high electronegativity of O from the oleate ligand. Following these new insights, by properly balancing the coordination of oleic acid and oleylamine to Mn^{2+}, the selective synthesis of MnO and Mn_3O_4 nanocrystals with uniform shapes was successfully achieved.

Introduction

Manganese oxides have drawn considerable interest owing to their potential applications in high-performance electrodes,[1] catalysts,[2,3] soft magnetic storage,[4] and contrast agents for magnetic resonance imaging.[5–7]

Over the past years, great efforts have been paid for regulating the sizes and shapes of manganese oxide nanocrystals synthesized through different wet-chemical synthetic routes.[8–10] Among them, pyrolyzing manganese-organic compounds at elevated temperature, known as the thermal decomposition method, has been demonstrated as the most effective approach for achieving high-quality manganese oxide nanocrystals.[11,12] In this method, oleylamine and oleic acid are widely used ligands for obtaining both regularly shaped rare-earth nanocrystals[13] and transition metal oxides.[14]

Owing to its high boiling point (b.p. ≈ 350 °C), oleylamine can be used as a coordinating solvent for manganese oxide nanocrystals. For example, by pyrolyzing $Mn(acac)_2$ (ref. 15 and 16) or $Mn(HCOO)_2$ (ref. 17) in oleylamine, monodispersed Mn_3O_4 nanocrystals in a size range of 6–15 nm were created. Alternatively, by using oleic acid instead of oleylamine as a surface capping agent, monodispersed MnO nanocrystals of 7–20 nm were obtained by pyrolyzing manganese(II) acetate ($Mn(Ac)_2$) in trioctylamine (TOA).[18] Through the reaction temperature and ratio of surface capping agent to precursor, MnO nanocrystals with various shapes such as nano-dumbbells and nano-crosses were also reported.[19,20] It is worth mentioning that pyrolyzing Mn–oleate solely in the presence of oleic acid or even in absence of any surface capping ligand generated not only monodispersed spherical MnO nanocrystals but also monodisperse MnO nanocrystals with different sizes and shapes.[21–24] Although the aforementioned thermal decomposition reactions were carried out in an inert atmosphere, oleylamine was found to favor the formation of Mn_3O_4,[25] while oleic acid tended to give rise to MnO.[22,26]

Very commonly, oleylamine and oleic acid were also used simultaneously as surface capping agents for synthesizing manganese oxide nanocrystals. But the form of the resulting manganese oxide particles was quite dependent on synthesis

---

[a] *Institute of Chemistry, Chinese Academy of Sciences, Bei Yi Jie 2, Zhong Guan Cun, Beijing 100190, China. E-mail: gaomy@iccas.ac.cn; Fax: +86-10-82613214; Tel: +86-10-82613214*

[b] *School of Radiation Medicine and Radiation Protection, Soochow University, 199 Ren-Ai Road, Suzhou Industrial Park, Suzhou 215123, China. E-mail: zhenli76820@yahoo.com*

† Electronic supplementary information (ESI) available: (1) TEM image and corresponding SAED pattern of the tiny particles shown in Fig. 1b; (2) TEM images of the branched nanoparticles (Fig. 1e) showing a self-organized superstructure; (3) TEM image and the electron diffraction pattern of the particles obtained by heating the $Mn(Ac)_2$ in oleylamine at 100 °C for 540 min; (4) TEM image and the electron diffraction pattern of the particles obtained from the second reference experiment; (5) Temporal evolution of size and size distribution of manganese oxide nanocrystals shown in Fig. 5 and Fig. 6. See DOI: 10.1039/c4nr00761a

parameters. For example, octahedral MnO nanocrystals were obtained through the thermal decomposition of $Mn(Ac)_2$ in TOA.[27] Both Mn_3O_4 and MnO nanocrystals were simultaneously formed upon the pyrolysis of $Mn(acac)_2$ in an inert atmosphere.[28] Mn_3O_4 nanocrystals were formed in air atmosphere upon the pyrolysis of $Mn(Ac)_2$.[29] Therefore it can be summarized that oleylamine and oleic acid as surface capping agents offer remarkable flexibility for preparing manganese oxides with tunable compositions through the thermal decomposition approach. Nevertheless, there remains a lack of in-depth studies into the underlying molecular mechanism for such ligand-dependent composition of manganese oxide nanocrystals.

Herein, we report the synthesis of manganese oxide nanocrystals through the thermal decomposition of $Mn(Ac)_2$ in 1-octadecene (ODE) by using oleylamine and oleic acid as surface capping agents. To disclose the surface ligand-dependent formation of MnO and Mn_3O_4 nanocrystals, different heating procedures were purposely implemented. In addition, various reference experiments were designed to show the effects of oleylamine and oleic acid in achieving different manganese oxide nanocrystals to facilitate discussion of the underlying mechanisms.

Experimental

Chemicals

The following materials were purchased from Sigma-Aldrich: $Mn(Ac)_2$ (330 825), oleylamine (O7805), oleic acid (364 525), and ODE (O806). $MnCl_2 \cdot 4H_2O$, sodium oleate, ethanol, cyclohexane, hexane, acetone, and tetrahydrofuran (THF) were purchased from Sinopharm Chemical Reagent Beijing, Co. Ltd. All chemicals were used as received without further purification. Mn–oleate was prepared according to a method previously reported.[21]

Synthesis of manganese oxide nanoparticles

In a typical synthesis, 0.3465 g (2 mmol) of $Mn(Ac)_2$, 6.4 mL (20 mmol) of oleylamine, and 6.3 mL (20 mmol) of oleic acid were mixed with 12.8 mL (40 mmol) of ODE in a 50 mL flask. The resulting mixture was continuously heated under nitrogen protection to 200 °C in 9 min and then to 250 °C by ~30 min. Aliquots were extracted at 250 °C at different reaction time periods to monitor the particle growth. The resulting nanoparticles were precipitated by acetone, collected by centrifugation, washed with acetone three times, and finally redispersed in THF or cyclohexane for further experiments.

The first reference experiment was carried out as follows. A preheating procedure was first implemented by maintaining the same stock solution as mentioned above at 100 °C for 60 min. Then, the reaction mixture was heated up to 250 °C at the same rate of temperature increase. Aliquots were also extracted at 250 °C to monitor the particle growth. The subsequent purification procedures were the same as those mentioned above.

The second reference experiment was carried out in a way that the same stock solution prepared by the recipe mentioned above was heated up to 250 °C in 17 min.

Post-treatment of branched MnO nanocrystals in oleylamine

The eight-arm MnO octapods were prepared through the first reference experiment in a reaction time of 20 min. After purification, 67 mg of the as-prepared MnO octapods were dispersed in 6.4 mL of oleylamine, and the resulting mixture was then heated to 250 °C. Aliquots were extracted to monitor the particle growth.

Determination of conversion yield

Concentrated HCl was used to dissolve the purified manganese oxide particles for determining the Mn content by inductively coupled plasma atomic emission spectroscopy (ICP-AES).

Characterization

Low-resolution transmission electron microscopy (TEM) images and electron diffraction patterns were recorded with a JEM-100CXII electron microscope operating at an accelerating voltage of 100 kV. High-resolution TEM (HRTEM) images and selected-area electron diffraction patterns (SAED) were taken on an FEI Tecnai 20 working at an accelerating voltage of 200 kV. Powder X-ray diffraction patterns were obtained with a Rigaku D/Max-2500 diffractometer equipped with a Cu-Kα1 source (λ = 1.54056 Å). The conversion yield of manganese oxides was determined by using an inductively coupled plasma atomic emission spectrometer (ICP-2000) produced by Jiangsu Skyray Instrument Co. Ltd. Fourier transform infrared (FTIR) spectra and UV-Vis absorption spectra of the reaction mixtures with different combinations of reactants were recorded on a Bruker EQUINOX55 FT-IR spectrometer and a Cary 50 UV-Vis absorption spectrometer respectively at room temperature.

Results

In a typical synthesis, $Mn(Ac)_2$, oleic acid, and oleylamine were dissolved in ODE at a molar ratio of 1 : 10 : 10. Under nitrogen atmosphere, the resulting mixture was heated up to 200 °C in 9 min and then to 250 °C by ~30 min without any interruption. It was observed that the reaction mixture became a yellow transparent solution at around 100 °C. Aliquots were extracted during the heating process at 250 °C to monitor the particle growth. As shown in Fig. 1a, tiny particles of ~2 nm are dominant at 10 min. However, larger particles in quasi-cubic shape start to appear. Further prolonging the reaction time to 20 min not only increases the size of small particles, but also changes the large particles into branched ones as shown in Fig. 1b. The electron diffraction patterns in Fig. 1c indicate that the particles are composed of tetragonal phase Mn_3O_4 and face-centered-cubic (fcc) phase MnO. Further SAED and HRTEM results, given in Fig. S1 in the ESI,† demonstrate that the tiny particles are of tetragonal Mn_3O_4 nanocrystals. Therefore, the large particles are probably fcc MnO nanocrystals.

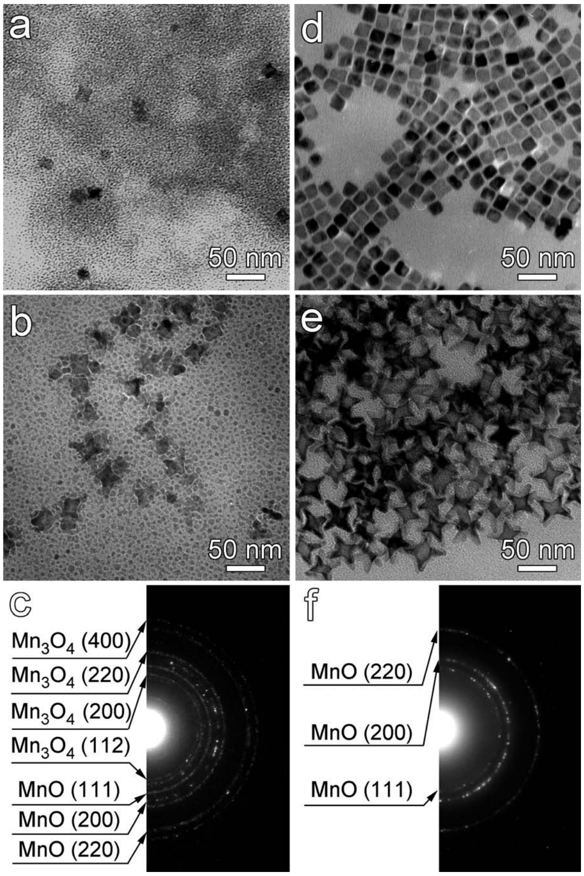

Fig. 1 TEM images of the particles obtained at reaction times of 10 min (a), 20 min (b) at 250 °C together with the electron diffraction patterns for the particles shown in Frame b (c), compared with those obtained by implementing the preheating procedure followed by reaction at 250 °C at 10 min (d), 20 min (e), and the electron diffraction pattern of the particles shown in Frame e (f). The diffraction rings are labeled with Miller indices according to fcc MnO (JCPDS 75-0626) and tetragonal Mn_3O_4 (JCPDS 24-0734), respectively.

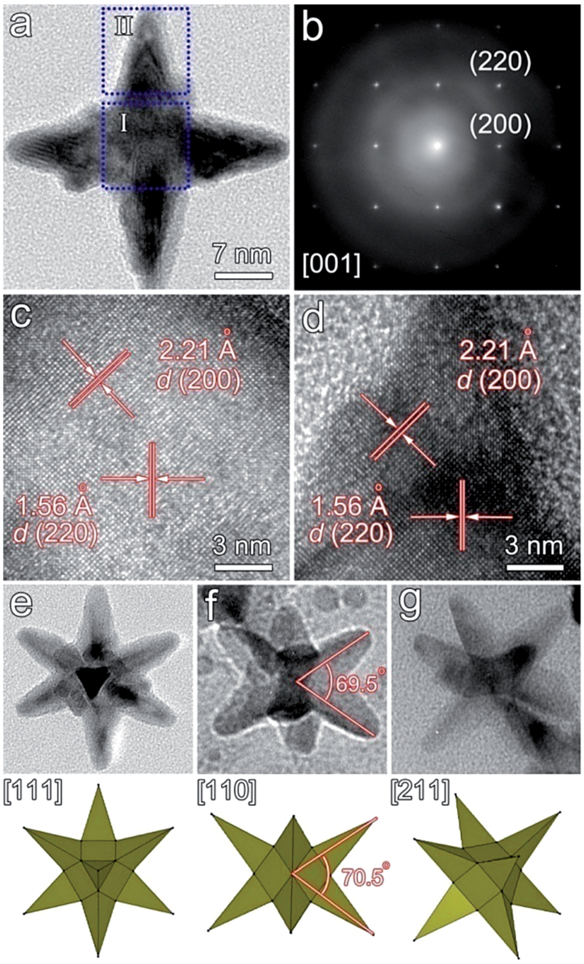

Fig. 2 A representative TEM image of a typical branched particle showing four arms (a) together with its electron diffraction pattern (b) and HRTEM images taken from the central (c) and arm (d) regions of the four-arm particle overlaid with crystal plane identifications according to JCPDS card (75-0626) for fcc MnO. Frames e–g present TEM images of the branched MnO particles showing different orientations for comparing with a model viewed from [111], [110], and [211] directions, as presented below.

In huge contrast, if the reaction mixture was kept under N_2 atmosphere for 60 min at 100 °C prior to the reaction at 250 °C, particles with significantly different sizes and shapes were obtained. As shown in Fig. 1d, 10 min of reaction at 250 °C leads to nanocubes that present preferential growth tendency from the corners and form star-like particles when the reaction is prolonged to 20 min (Fig. 1e). In combination with results shown in Fig. 1d and e, it can be concluded that the star-like particles are formed *via* an overgrowth process rather than an etching process as previously reported.[27] The electron diffraction patterns shown in Fig. 1f demonstrate that the star-shaped particles are of fcc MnO nanocrystals.

As shown in Fig. S2 in ESI,† the four-arm stars with higher contrast at the arm regions also appeared as six-arm stars in some locations of the same TEM grid and even formed self-organized superstructures. To further determine the overall structure of crystalline nanostars for better understanding their formation mechanism, TEM and HRTEM investigations were carried out. Fig. 2a presents a particle showing a typical four-arm configuration. The SAED pattern shown in Fig. 2b confirms that the nanostar is a single crystal of fcc MnO. The assignments of the diffraction dots suggest that the four-arm star shown in Fig. 2a is a zone axis projection image along [001], which is supported by the HRTEM results in Fig. 2c and d taken from the central (I) and arm (II) regions of the four-arm star, respectively. The detailed analysis provided in Fig. 2c and d not only supports the single crystal structure of the four-arm star, but also verifies its orientation on the TEM grid. Because fcc nanocubes in Fig. 1d possess a highly symmetric structure enveloped by identical {100} planes, the further growth will give rise to six arms along [001] directions or eight arms if along [111] directions. Nevertheless, the highest contrast is observed at the central part of a nanostar showing six arms (Fig. 2e); thus, it can be deduced that the nanostar may possess an octapod structure. To verify this hypothesis, the nanostars presenting different orientations were carefully imaged and compared with an octapod model as illustrated in Fig. 2e–g. The particles match perfectly with the model representing an fcc crystal with eight epitaxial arms growing along the [111] directions, viewed from the [111], [110], and [211] directions, respectively. In addition, the angle between two adjacent arms, *i.e.*, 69.5°, is also consistent with the theoretical angle between [111] and [11$\bar{1}$], *i.e.*, 70.5°, further proving that the arms grow from the corners of the nanocubes along the [111] directions.

Discussion

All the aforementioned results reveal the following two facts for the formation of manganese oxide nanoparticles through the pyrolysis of $Mn(Ac)_2$ in the presence of oleic acid and oleylamine: (1) by continuously heating the reaction mixture up to 250 °C, the following reaction leads to a mixture of spherical Mn_3O_4 particles and branched MnO particles; (2) the preheating process at 100 °C, however, leads to the formation of pure MnO nanocubes that are altered into regular eight-arm MnO nanostars upon prolonged reaction at elevated temperature. In other words, the preheating process not only changes the morphology, but also the form of the resulting manganese oxide particles. Therefore, the manner in which the preheating process changes the morphology and form of the resulting manganese oxide nanoparticles is an important topic.

Mechanisms for forming manganese oxide nanocrystals with different morphologies

With respect to the formation of branched nanocrystals, previous studies on semiconductor nanocrystals suggest that branched structures are prone to form at temperatures lower than that required for forming low-dimensional particles.[30,31] For example, out of the reaction system generating MnS nanocubes at 200 °C, MnS tetrapods were obtained at 120 °C.[32] Similarly, CdS bipods were formed at 120 °C due to the epitaxial growth of wurtzite pods from the {111} facets, contrasting to CdS nanorods formed at ∼300 °C.[33] The underlying mechanisms for achieving such shape variations are believed to be related to the pyrolytic behavior of the precursors at different temperatures[34] and can generally be understood as follows. Lowering the reaction temperature undoubtedly reduces the monomer supply rate, which encourages the monomer to grow on pre-existing particles rather than forming new nuclei. A preferential epitaxial growth from certain facets will then give rise to branched nanocrystals.

In fact, it was previously reported that the involvement of surface ligands in the pyrolysis of metal precursors can alter the particle growth kinetics.[35,36] Although oleic acid and oleylamine are commonly used surface ligands for nanometer-sized transition metal oxides and show remarkable flexibility in regulating the shapes and compositions of manganese oxide nanocrystals, their effect on the pyrolytic behaviors of Mn precursors has not been reported thus far. To disclose the impacts of oleic acid and oleylamine on the pyrolysis of $Mn(Ac)_2$ precursor, the following experiments were carried out to show the differences in the coordination chemistry of oleylamine and oleic acid with Mn^{2+}.

The first experiment was carried out as follows. $Mn(Ac)_2$ was mixed with oleylamine at a molar ratio of 1 : 10. The resulting mixture was then heated up to 100 °C under nitrogen protection and maintained at this temperature for 600 min under stirring. It was observed that the powder of $Mn(Ac)_2$ immediately changed in color from shallow pink to brown after oleylamine was introduced. The resulting reaction mixture then quickly formed a homogeneous black solution when the solution temperature reached 80 °C, suggesting that oleylamine can quickly bind to Mn^{2+} to assist the dissolution of $Mn(Ac)_2$ that is hardly dissolved in ODE. During the subsequent heating process, the reaction mixture remained nearly unchanged in color, which can be seen from the photographs of the aliquots extracted at 80 °C (solution 1) and after heating to 100 °C for 0 min (solution 2), 60 min (solution 3), 180 min (solution 4) and 300 min (solution 5) (Fig. 3a). FTIR spectroscopy studies reveal that the $-NH_2$ symmetric stretch vibration of oleylamine at 3318 cm^{-1} is greatly reduced in intensity after $Mn(Ac)_2$ is dissolved, as shown in Fig. 3b, because oleylamine readily donates its lone pair of electrons to Mn^{2+} to form the Mn^{2+}–oleylamine

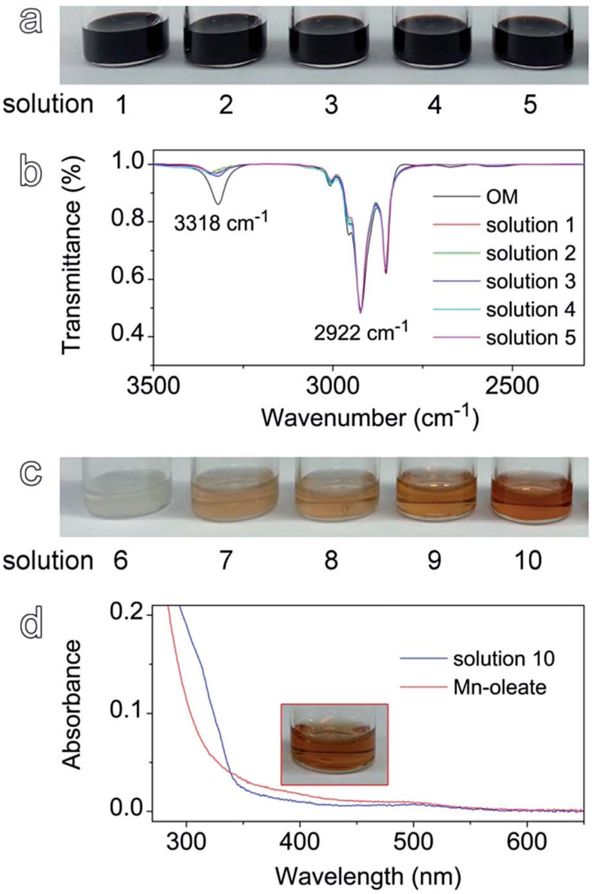

Fig. 3 (a) Photographs of solutions 1–5 formed by $Mn(Ac)_2$ and oleylamine. (b) FTIR spectra of solutions 1–5 together with that of oleylamine normalized according to the absorbance at 2922 cm^{-1}. (c) Photographs of solutions 6–10 formed by $Mn(Ac)_2$ and oleic acid. (d) UV-Vis absorption spectra of solution 10 for comparing with that recorded from the cyclohexane solution containing Mn–oleate. Inset: photograph of the Mn–oleate solution.

complex.[16,37–39] It is worth mentioning that a 9 h reaction at 100 °C eventually led to quasi cubic Mn_3O_4 nanoparticles of ~8 nm, as shown in Fig. S3 in the ESI.† Although the resulting Mn_3O_4 nanoparticles are larger than those presented in Fig. 1b, the above results strongly support the theory that oleylamine favors the formation of Mn_3O_4 nanoparticles. Moreover, the greatly reduced reaction temperature, *i.e.*, 100 °C, obviously facilitated the crystal growth from certain facets though Mn_3O_4 nanocubes rather than branched formation.

The second experiment was performed for investigating the coordination between oleic acid and Mn^{2+}. In brief, $Mn(Ac)_2$ was mixed with oleic acid also at a molar ratio of 1 : 10. The resulting mixture was subjected to the same heating treatment as mentioned above at 100 °C. The aliquots were extracted at 80 °C (solution 6) and after heating to 100 °C for 0 min (solution 7), 60 min (solution 8), 180 min (solution 9) and 300 min (solution 10). The photographs of solutions 6–10 shown in Fig. 3c reveal that $Mn(Ac)_2$ remains in powder form at 80 °C (solution 6) but starts to be dissolved when the solution temperature reaches 100 °C, giving rise to a turbid shallow brown colored dispersion (solution 7). The reaction mixture eventually forms a homogeneous brown solution after 300 min at 100 °C. The color of solution 10 strongly resembles that of a cyclohexane solution of Mn–oleate with the same concentration of Mn^{2+} (inset of Fig. 3d). Thereafter, the solution color remained nearly unchanged upon prolonged heating treatment. The absorption spectroscopy results shown in Fig. 3d imply that Mn–oleate is formed upon the substitution of the acetate group of $Mn(Ac)_2$ by an oleate group, which is also supported by the fact that gaseous acetic acid was continuously released during the heating treatment.

In brief, the above two experiments demonstrate that oleylamine as a coordinating agent can quickly bind to Mn^{2+} and that the resulting complex can even be thermally decomposed at 100 °C to form Mn_3O_4 nanoparticles. Although oleic acid can replace the acetate group of $Mn(Ac)_2$ to form Mn–oleate, the kinetics are much slower. In addition, the same heating treatment at 100 °C does not decompose Mn–oleate. Nevertheless, Mn–oleate can be decomposed at higher temperature in solvents such as ODE yielding pure fcc MnO nanocrystals.[21] In addition, the above experiments also suggest that the coordination with oleylamine is more kinetically favorable than oleic acid to Mn^{2+}.

To show competitive coordination of oleic acid and oleylamine with Mn^{2+}, absorption spectroscopy studies were carried out. As shown in Fig. 4, the absorption of the stock solution containing $Mn(Ac)_2$, oleylamine and ODE covers almost the entire ultraviolet-visible range with greatly enhanced intensity below 350 nm due to the formation of Mn^{2+}–oleylamine complex. In contrast, the stock solution for preparing the particles shown in Fig. 1 presents greatly decreased absorbance. Moreover, the heating process at 100 °C gradually decreases the overall absorption and eventually makes the absorption spectrum of the stock solution approach that recorded from the mixture of $Mn(Ac)_2$, oleic acid, and ODE. This strongly supports the theory that the preheating process gradually transforms the oleylamine-dominant coordination to oleic acid-dominant coordination to Mn^{2+}, suggesting that the latter is more thermodynamically stable. According to hard and soft acids and bases (HSAB) theory, Mn^{2+} is a hard acid, whereas deprotonated oleic acid and oleylamine are hard bases. However, the deprotonated oleic acid presents stronger hardness than oleylamine. Therefore, the Mn^{2+}–oleate is more stable than Mn^{2+}–oleylamine, which explains the formation of eight-arm MnO nanocrystals resulting from the preheating procedure because the oleic acid-dominant complex greatly reduces the monomer supplying rate for forming manganese oxide.

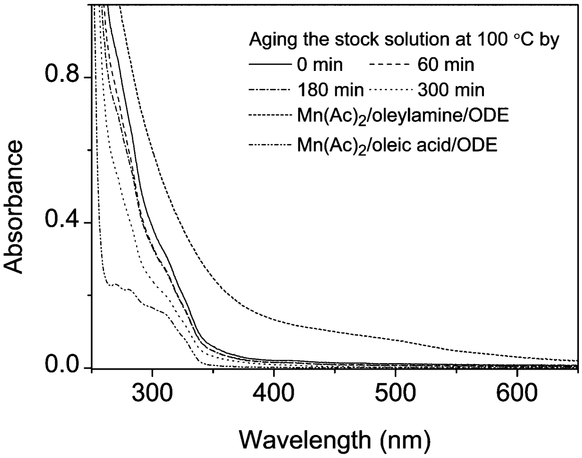

Fig. 4 UV-Vis absorption spectra of the stock solution containing $Mn(Ac)_2$, oleylamine, oleic acid, and ODE, recorded after being treated at 100 °C for 0, 60, 180 and 300 min, respectively, for comparing with those recorded from the reference solutions. The reference solution of $Mn(Ac)_2$–oleylamine–ODE was prepared by heating the reaction mixture to 80 °C to dissolve $Mn(Ac)_2$, while the reference solution of $Mn(Ac)_2$–oleic acid–ODE was prepared by heating the reaction mixture at 100 °C for 300 min to completely dissolve $Mn(Ac)_2$.

Mechanisms for forming manganese oxide nanocrystals of different forms

According to previous studies, oleylamine favors the formation of Mn_3O_4, whereas oleic acid is favorable for the formation of MnO.[15,16,18,22] Therefore, the formation of MnO nanocubes and octapods may be explained by the transformation of an oleylamine-dominant system to an oleic acid-dominant system owing to the preheating process. To further verify this hypothesis, a control experiment was carried out by quickly heating a reference stock solution containing $Mn(Ac)_2$, oleic acid, and oleylamine up to 250 °C within 17 min in order to minimize the transformation of Mn^{2+}–oleylamine to Mn^{2+}–oleate. The results shown in Fig. S4† revealed that spherical Mn_3O_4 particles with an average size of 4.2 nm were formed after 20 min reaction at 250 °C. Thus, properly balancing the kinetics for forming molecular complexes involving oleylamine and oleic acid can give rise to different forms of manganese oxide nanocrystals. Thus, the commonly used ligand pair of oleylamine and oleic acid offers a molecular switch for changing the chemical environment of the manganese precursor, which largely determines the oxidation state of manganese in the resulting nanomaterials.

Regarding the oxidation state of manganese in the resulting oxides, it is well-known that the redox potentials of manganese ions in an aqueous solution are quite dependent on the pH. The standard reduction potential of Mn^{3+}/Mn^{2+} in basic media is around −0.25 V, which is much more negative than 1.5 V in acidic media.[40] In other words, Mn^{2+} is more readily oxidized to Mn^{3+} in basic media. In addition, O has higher electronegativity than N,[41] and Mn^{2+}–oleylamine is more prone to be oxidized than Mn^{2+}–oleate in non-aqueous solutions, which implies the expectation of MnO formation upon the introduction of the preheating procedures. Regarding the formation of the mixture of MnO and Mn_3O_4 nanocrystals, when no preheating procedure is implemented, the formation of Mn_3O_4 is mainly caused by the incomplete transformation of Mn^{2+}–oleylamine to Mn^{2+}–oleate. In this context, by properly balancing the competitive coordination of oleylamine/oleic acid to Mn^{2+}, Mn_3O_4 nanocrystals may also be obtained even in the presence of oleic acid because it will be thermally decomposed to supply O in forming manganese oxides.

To demonstrate the feasibility of producing pure Mn_3O_4 nanocrystals, the reaction time for the system yielding the eight-arm MnO nanocrystals shown in Fig. 1e was further prolonged. As shown in Fig. 5a, 6.3 ± 0.9 nm spherical nanoparticles start to appear at 30 min and are identified as tetragonal Mn_3O_4 nanocrystals according to the inset of Fig. 5a. The regular branched particles remain dominant with the average size increasing from 45.4 ± 3.8 nm (20 min) to 52.7 ± 5.4 nm (30 min). Further prolonging the reaction time to 60 min destroys the branched particles. At the same time, the number of Mn_3O_4 nanocrystals with bigger size, as shown in Fig. 5b, apparently increases. Following these tendencies, the branched MnO particles completely vanish at 600 min, and the small particles further grow in size to form uniform spherical Mn_3O_4 nanocrystals of 8.7 ± 1.1 nm, as shown in Fig. 5c. The powder X-ray diffraction results exhibited in Fig. 5d suggest that MnO particles are completely transformed into Mn_3O_4 by the prolonged reaction time. However, the manner in which the spherical Mn_3O_4 particles are formed remains an open question.

According to the results shown in Fig. 5, the branched eight-arm MnO particles undergo growth in size until 30 min followed by degradation upon further reaction at 250 °C. To disclose the correlation between the formation of Mn_3O_4 nanocrystals and the degradation of the branched MnO particles, the as-prepared eight-arm MnO particles obtained by 20 min of reaction were collected, purified, and then dispersed in ODE containing oleylamine. The reaction mixture was then quickly heated up to 250 °C, and aliquots were extracted for monitoring the morphological changes of the eight-arm MnO particles against the reaction time, *i.e.*, 0, 60, 180, and 600 min. As shown in Fig. 6, the heating treatment of the eight-arm MnO particles gradually destroys the branched particles to give rise to spherical Mn_3O_4 nanocrystals that are smaller than those shown in Fig. 5c. This strongly indicates that the oleylamine dominant reaction environment on the one hand can degrade the branched MnO nanoparticles, while on the other hand leads to the oxidation of MnO to form Mn_3O_4. Nevertheless, the results shown in Fig. 5a also reveal that tiny Mn_3O_4 nanoparticles have already been formed from the reaction system yielding eight-arm MnO nanoparticles before the degradation of the branched MnO particles. Therefore, it can be deduced that a portion of the Mn_3O_4 nanocrystals are formed independent of the degradation of the branched MnO particles. The detailed information

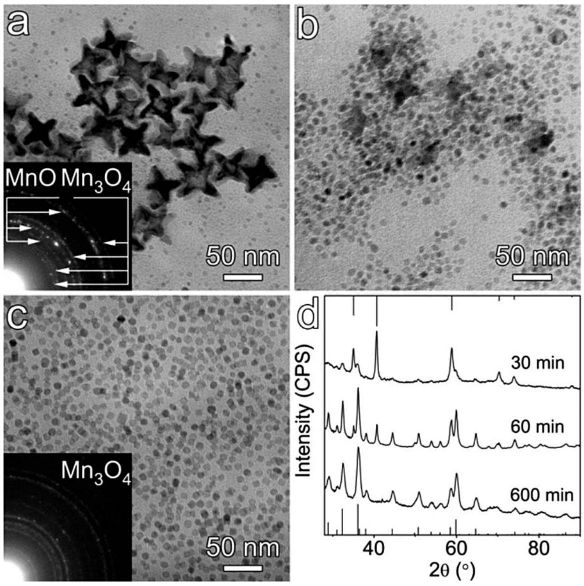

Fig. 5 TEM images of the particles obtained by prolonging the reaction yielding the particles shown in Fig. 1e to 30 (a), 60 (b), and 600 min (c), at 250 °C, and powder X-ray diffraction patterns of the resulting nanoparticles (d). Insets: electron diffraction patterns labeled with Miller indices according to fcc MnO (JCPDS 75-0626) and tetragonal Mn_3O_4 (JCPDS 24-0734), respectively. The bottom and top line patterns drawn in (d) show standard data for Mn_3O_4 and MnO, respectively.

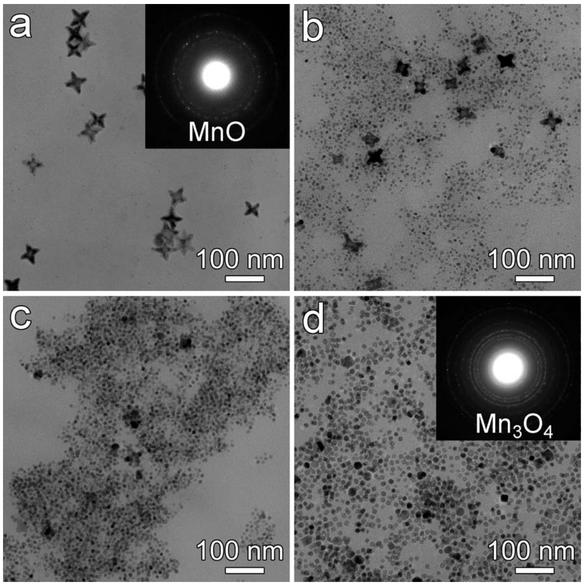

Fig. 6 TEM images of the branched MnO nanoparticles after being treated at 250 °C in ODE containing oleylamine for 0 (a), 60 (b), 180 (c), and 600 min (d), respectively. Insets: electron diffraction patterns of the corresponding particles.

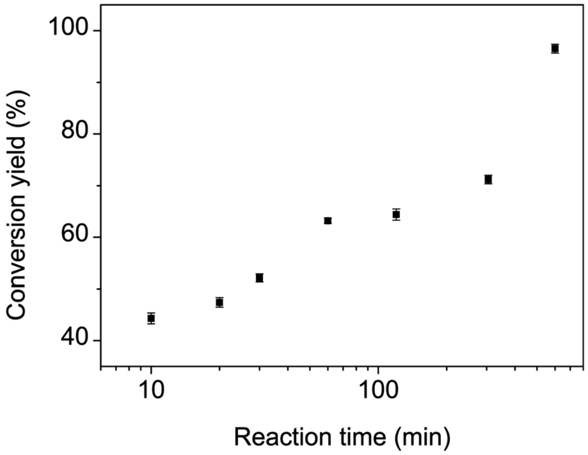

Fig. 7 Temporal conversion yield for manganese oxide nanoparticles formed in the presence of oleic acid and oleylamine. The error bars are derived from three parallel measurements for determining the Mn content.

on size distribution of the particles shown in Fig. 5 and 6 are provided in Fig. S5 and S6.†

The temporal conversion of manganese oxide particles shown in Fig. 7 reveals that the conversion yield for generating the eight-arm MnO nanocrystals at 20 min is only of 47.4 ± 0.9%. The value is slightly increased to 52.1 ± 0.8% by 30 min upon the formation of Mn_3O_4 before the branched MnO nanoparticles are broken down. Following the degradation of the branched MnO and independent formation of Mn_3O_4, the conversion yield is gradually increased and reaches nearly 96.5 ± 0.9% by 600 min, yielding the uniform Mn_3O_4 particles shown in Fig. 5c.

Based on the results presented in Fig. 3 and 4, it can be concluded that the preheating procedure can gradually shift the reaction system from oleylamine-dominant to oleic acid-dominant, which favors formation of branched MnO nanoparticles. Nevertheless, along with the degradation of the oleate ligand upon prolonged reaction, the system becomes oleylamine-dominant again. This not only encourages the formation of Mn_3O_4 nanocrystals, but also transforms the branched MnO nanoparticles into Mn_3O_4 particles.

Conclusions

In summary, the preparation of nanocrystals of manganese oxides by pyrolyzing $Mn(Ac)_2$ in ODE in the presence of oleylamine and oleic acid was investigated. Detailed studies reveal that both oleylamine and oleic acid can coordinate to Mn^{2+} but present different behaviors, *i.e.*, the formation of Mn^{2+}–oleylamine is more kinetically favorable, while the formation of Mn^{2+}–oleate is more thermodynamically favorable. Since Mn^{2+} is more prone to be oxidized upon coordination with oleylamine than with oleate, the heating procedures play a determining role in selective synthesis of MnO and Mn_3O_4 nanocrystals by balancing the coordination of oleylamine/oleic acid to Mn^{2+}. In brief, the current investigations provide deeper understanding on the roles of oleic acid and oleylamine, which are commonly used surface ligands for preparing transition metal oxide nanocrystals.

Acknowledgements

The authors thank the National Basic Research Program of China (2011CB935800), the National Nature Science Foundation of China (81090271, 21203210, 21203211 and 21021003), and ICCAS (CMS-PY-201309) for financial support. The authors also thank Dr Ivan Kempson for stimulating discussion.

Notes and references

1 A. R. Armstrong and P. G. Bruce, *Nature*, 1996, **381**, 499.
2 G. H. Qiu, H. Huang, S. Dharmarathna, E. Benbow, L. Stafford and S. L. Suib, *Chem. Mater.*, 2011, **23**, 3892.
3 C. Chen, G. Ding, D. Zhang, Z. Jiao, M. Wu, C.-H. Shek, C. M. L. Wu, J. K. L. Lai and Z. Chen, *Nanoscale*, 2012, **4**, 2590.
4 A. H. de Vries, L. Hozoi, R. Broer and P. S. Bagus, *Phys. Rev. B: Condens. Matter Mater. Phys.*, 2002, **66**, 035108.
5 H. B. Na, J. H. Lee, K. J. An, Y. I. Park, M. Park, I. S. Lee, D. H. Nam, S. T. Kim, S. H. Kim, S. W. Kim, K. H. Lim, K. S. Kim, S. O. Kim and T. Hyeon, *Angew. Chem., Int. Ed.*, 2007, **46**, 5397.
6 U. I. Tromsdorf, N. C. Bigall, M. G. Kaul, O. T. Bruns, M. S. Nikolic, B. Mollwitz, R. A. Sperling, R. Reimer, H. Hohenberg, W. J. Parak, S. Forster, U. Beisiegel, G. Adam and H. Weller, *Nano Lett.*, 2007, **7**, 2422.
7 R. J. Xing, G. Liu, Q. M. Quan, A. Bhirde, G. F. Zhang, A. Jin, L. H. Bryant, A. Zhang, A. Liang, H. S. Eden, Y. L. Hou and X. Y. Chen, *Chem. Commun.*, 2011, **47**, 12152.
8 Z. W. Chen, Z. Jiao, D. Y. Pan, Z. Li, M. H. Wu, C. H. Shek, C. M. L. Wu and J. K. L. Lai, *Chem. Rev.*, 2012, **112**, 3833.
9 T. Ahmad, K. V. Ramanujachary, S. E. Lofland and A. K. Ganguli, *J. Mater. Chem.*, 2004, **14**, 3406.
10 G. Salazar-Alvarez, J. Sort, S. Surinach, M. D. Baro and J. Nogues, *J. Am. Chem. Soc.*, 2007, **129**, 9102.
11 Y. F. Chen, E. Johnson and X. G. Peng, *J. Am. Chem. Soc.*, 2007, **129**, 10937.
12 Y. Tan, L. Meng, Q. Peng and Y. Li, *Chem. Commun.*, 2011, **47**, 1172.
13 H.-X. Mai, Y.-W. Zhang, R. Si, Z.-G. Yan, L.-d. Sun, L.-P. You and C.-H. Yan, *J. Am. Chem. Soc.*, 2006, **128**, 6426.
14 S. Sun and H. Zeng, *J. Am. Chem. Soc.*, 2002, **124**, 8204.
15 W. S. Seo, H. H. Jo, K. Lee, B. Kim, S. J. Oh and J. T. Park, *Angew. Chem., Int. Ed.*, 2004, **43**, 1115.
16 F. Jiao, A. Harrison and P. G. Bruce, *Angew. Chem., Int. Ed.*, 2007, **46**, 3946.
17 X. Sun, Y.-W. Zhang, R. Si and C.-H. Yan, *Small*, 2005, **1**, 1081.
18 M. Yin and S. O'Brien, *J. Am. Chem. Soc.*, 2003, **125**, 10180.
19 X. H. Zhong, R. G. Xie, L. T. Sun, I. Lieberwirth and W. Knoll, *J.Phys. Chem. B*, 2006, **110**, 2.
20 T. Ould-Ely, D. Prieto-Centurion, A. Kumar, W. Guo, W. V. Knowles, S. Asokan, M. S. Wong, I. Rusakova, A. Luttge and K. H. Whitmire, *Chem. Mater.*, 2006, **18**, 1821.

21 J. Park, K. J. An, Y. S. Hwang, J. G. Park, H. J. Noh, J. Y. Kim, J. H. Park, N. M. Hwang and T. Hyeon, *Nat. Mater.*, 2004, **3**, 891.

22 D. Zitoun, N. Pinna, N. Frolet and C. Belin, *J. Am. Chem. Soc.*, 2005, **127**, 15034.

23 K. An, M. Park, J. H. Yu, H. B. Na, N. Lee, J. Park, S. H. Choi, I. C. Song, W. K. Moon and T. Hyeon, *Eur. J. Inorg. Chem.*, 2012, **12**, 2148.

24 T. D. Schladt, T. Graf and W. Tremel, *Chem. Mater.*, 2009, **21**, 3183.

25 P. Li, C. Y. Nan, Z. Wei, J. Lu, Q. Peng and Y. D. Li, *Chem. Mater.*, 2010, **22**, 4232.

26 K. An, S. G. Kwon, M. Park, H. B. Na, S.-I. Baik, J. H. Yu, D. Kim, J. S. Son, Y. W. Kim, I. C. Song, W. K. Moon, H. M. Park and T. Hyeon, *Nano Lett.*, 2008, **8**, 4252.

27 T. Kim, E. J. Cho, Y. Chae, M. Kim, A. Oh, J. Jin, E. S. Lee, H. Baik, S. Haam, J. S. Suh, Y. M. Huh and K. Lee, *Angew. Chem., Int. Ed.*, 2011, **50**, 10589.

28 H. L. Si, H. Z. Wang, H. B. Shen, C. H. Zhou, S. Li, S. Y. Lou, W. W. Xu, Z. L. Du and L. S. Li, *CrystEngComm*, 2009, **11**, 1128.

29 T. Yu, J. Moon, J. Park, Y. I. Park, H. Bin Na, B. H. Kim, I. C. Song, W. K. Moon and T. Hyeon, *Chem. Mater.*, 2009, **21**, 2272.

30 L. Manna, D. J. Milliron, A. Meisel, E. C. Scher and A. P. Alivisatos, *Nat. Mater.*, 2003, **2**, 382.

31 Z. A. Peng and X. Peng, *J. Am. Chem. Soc.*, 2002, **124**, 3343.

32 Y.-W. Jun, Y.-Y. Jung and J. Cheon, *J. Am. Chem. Soc.*, 2002, **124**, 615.

33 Y.-W. Jun, S.-M. Lee, N.-J. Kang and J. Cheon, *J. Am. Chem. Soc.*, 2001, **123**, 5150.

34 Y. W. Jun, J. S. Choi and J. Cheon, *Angew. Chem., Int. Ed.*, 2006, **45**, 3414.

35 Q. J. Jia, J. F. Zeng, R. R. Qjao, L. H. Jing, L. Peng, F. L. Gu and M. Y. Gao, *J. Am. Chem. Soc.*, 2011, **133**, 19512.

36 W. Han, L. X. Yi, N. Zhao, A. W. Tang, M. Y. Gao and Z. Y. Tang, *J. Am. Chem. Soc.*, 2008, **130**, 13152.

37 W. B. Bu, Z. X. Chen, F. Chen and J. L. Shi, *J. Phys. Chem. C*, 2009, **113**, 12176.

38 M. Kar, R. Agrawal and H. W. Hillhouse, *J. Am. Chem. Soc.*, 2011, **133**, 17239.

39 Y. Li, J. Liu, Y. Wang and Z. L. Wang, *Chem. Mater.*, 2001, **13**, 1008.

40 M.-N. Collomb and A. Deronzier, in *Encyclopedia of Inorganic Chemistry*, John Wiley & Sons, Ltd, 2006, DOI: 10.1002/0470862106.ia126.

41 H. Chen, J. W. Faller, R. H. Crabtree and G. W. Brudvig, *J. Am. Chem. Soc.*, 2004, **126**, 7345.